Published in final edited form as:
Proc IEEE Int Symp Biomed Imaging. 2013 ; : 121–124. doi:10.1109/ISBI.2013.6556427.

MORPHOMETRY FOR EARLY MONITORING OF TREATMENT RESPONSE IN RHEUMATOID ARTHRITIS

Anand A. Joshi[1], **Richard M. Leahy**[1], **Ramsey D. Badawi**[2], and **Abhijit J. Chaudhari**[2]

[1]Signal and Image Processing Institute, University of Southern California, Los Angeles, CA 90089, USA

[2]Radiology, UC Davis School of Medicine, Sacramento, CA 95817, USA

Abstract

New aggressive therapeutic options have recently become available to treat inflammatory arthritis (IA) and rheumatoid arthritis in particular. These treatments not only control joint destruction, they may also aid in new bone formation at sites of eroded bone. Separation of non-responders from responders to these treatments, is critical, and is known to lead to reduced disease burden, toxicity, side-effects and overall cost. The bones of the wrist are early targets of IA and are known to show response to therapy early. In this paper, we develop a method to quantify point-wise erosive changes of wrist bones in IA patients undergoing treatment. The method employs 3D registration-based morphometric analysis. Our results indicate that the proposed method has potential to improve sensitivity to small, early changes in bone erosion status. This study has potential to provide new imaging biomarkers to be used in clinical trials evaluating the efficacy of new arthritis drugs.

1. INTRODUCTION

Inflammatory arthritis (IA), such as Rheumatoid Arthritis, is known to cause significant disability and loss of function. Over 2% of the world's population is affected by such conditions, 75% of whom are women [1]. IA also increases the risk for other diseases, such as cardiovascular and renal disease[2].

New aggressive biologic drugs (e.g., etanercept, infliximab) are proving to be highly effective for the treatment of IA [3]. These therapies not only control disease; data show that regeneration of eroded bone, and therefore recovery of function, is also possible. Determination of the right treatment for IA on an individual patient basis early in the disease cycle is becoming critical with the advent of new drugs [4] because of potentially severe side-effects.

The small joints of the wrist are typically one of the first areas to show response to biologic therapy [5]. Conventional techniques for measuring IA status, progression and response to therapy are physical examination by a rheumatologist or planar X-ray radiography. Tomographic imaging using X-ray CT or MRI is becoming increasingly common to overcome the limitations associated with subjectivity, poor sensitivity, and sub-optimal visualization capabilities of the conventional techniques. There is therefore demand for developing software tools that have high sensitivity to small, early changes in bone status, while allowing superior performance for interreader reproducibility and reliability than human observers [6].

In this paper we describe a method for performing morphometric *change analyses* on longitudinally-acquired high resolution anatomical images (X-ray CT and MRI) of the

carpal bones of the human arthritic wrist. Morphometric analyses are well-suited for the task of determining therapeutic efficacy in IA because bone destruction due to IA typically manifests as surface atrophy on carpal bones and results in a reduction in bone volume. A good response to a drug corresponds to bone remodeling and re-growth, hence, stable or increased bone volume. Localization of the change on the bone surface is also required since the distribution of erosive changes may be different for the different arthritides [7]. The technique developed here, registration-based morphometry, attempts to provide 3D maps of erosive changes in a longitudinal setting. We conduct initial validation of the technique on CT and MRI wrist scans in four IA patients undergoing treatment where the clinical outcome is known.

2. MATERIALS AND METHODS

2.1. Patient imaging data

Two patients with established IA who were candidates for starting the tumor necrosis factor-α blocker etanercept underwent hand X-ray CT scanning at baseline (a mean of 3 days before initiation of therapy) and at 90±7 days after starting treatment with 6 month follow up. Written informed consent was obtained based on the guidelines of the UC Davis Institutional Review Board. The characterization of the extremity CT system has been reported by our group previously [8]. Briefly, the patient lies prone on a table top and suspends his/her dominant hand into the CT field-of-view through a hole on the table top (Fig. 1(a)). The CT field-of-view is 15 cm. At 30 frames/s, 500 cone-beam projection images were acquired at 360° around the patient's hand in 17 s. Images were reconstructed into a 512 × 512 × 512 matrix with an isotropic voxel size of 0.3 mm using the Feldkamp method. To limit intra- and inter-scan movement and repositioning error, a CT-compatible patient-specific hand immobilizer was designed (fabrication time <5 min) from thermoplastic materials and reused for longitudinal follow-up (Fig. 1(b)). The thermoplastic material was MR-compatible.

In a separate study, two different patients with the same characteristics as above underwent MRI scanning of the hand on a General Electric 1.5T MRI scanner, using the knee coil and the thermoplastic mold (Fig. 1(c)). T_1-weighted images of the wrist of the dominant hand were acquired with a 0.5 mm isotropic voxel size at baseline and at 90±7 days after initiation of treatment.

2.2. Morphometric analysis for change detection

In order to perform point-wise measurements of volumetric change, the triangulated representations of the boundaries of the segmented regions were extracted for a single bone in the baseline and follow-up scans. These surfaces were then registered using a surface-based registration method (section 2.2.1) and the point-wise measure was computed.

2.2.1. Surface-based registration—The matching problem for registering the boundary triangulations of bone surfaces was formulated as an L^2 distance minimization, where the distance was computed from the pointset of the bone surface from baseline (template) to that from follow-up (target). The L^2 distance metric d between the template $\partial\Omega_A$ and target surface $\partial\Omega_S$ was defined by:

$$d(\partial\Omega_A, \partial\Omega_S) = \sqrt{\sum_{p\in\partial\Omega_A}\left(\inf_{e\in\partial\Omega_S}\|p-e\|^2\right)^2} + \sqrt{\sum_{p\in\partial\Omega_S}\left(\inf_{e\in\partial\Omega_A}\|p-e\|^2\right)^2}$$

In this expression, for each location on the target surface point-set we find the closest point on the template surface and vice-versa. Our objective, then, was to deform the template surface $\partial\Omega_A$ such that the distance metric is minimized. Additionally, we wanted the displacement field for this operation U to be smooth, such that the deformed surface $\partial\Omega_A + U$ remained smooth. This was achieved by a Laplacian regularizer on the displacement field. The cost function C_S was defined as:

$$C_S(U) = d(\partial\Omega_S, \partial\Omega_A + U)^2 + \|\Delta_d U\|^2,$$

where Δ_d denotes the discrete Laplacian [9] calculated on the triangulated mesh of the boundary. The minimization of the pseudo-distance was performed by a search strategy over the point-set and gradient descent [10], and resulted in a displacement vector field U. The search algorithm was based on the Qhull algorithm and was implemented in MATLAB®. The displacement field U obtained as a result of this minimization was then applied to the template surface $\partial\Omega_A$ to get the surface $\partial\Omega_S = \partial\Omega_A + U$ that matched the target surface $\partial\Omega_S$.

2.2.2. A point-wise measure of volumetric change—The application of the L^2-based surface registration process yields a point-wise displacement vector field at every point on the mesh model of the bone. However, the real interest here was to compute the amount of bone change at various points on the surface. A point-wise measure of volume change was necessary for such a characterization. Here we present such a measure based on surface warping [11].

First, we computed a Voronoi tessellation of the given polyhedral mesh. A Voronoi cell R_k for node P_k consists of all points on the polyhedral mesh whose distance to P_k is not greater than their distance to any other node. A depiction of a Voronoi cell corresponding to a node is shown in Fig. 3. The Voronoi tessellation resulted in a decomposition of the polyhedral mesh into Voronoi cells, such that each cell corresponded to the node that lies at its center. For a triangular mesh, area of the Voronoi cells can be computed in closed form by

$$A_{\text{Voronoi}} = \frac{1}{8} \sum_{j \in N_1(i)} \left(\cot\alpha_{ij} + \cot\beta_{ij}\right) \|x_i - x_j\|^2,$$

where $N_1(i)$ denotes the ring of vertices that directly connect vertex i. In order to get a measure of the point-wise volume change D_{Vol}, we multiplied the area of the Voronoi cell for the vertex i denoted by A_{Voronoi} by the displacement d computed at i:

$$D_{\text{Vol}} = A_{\text{Voronoi}} \cdot d$$

This was a point-wise measure of the volume change defined at nodes of the triangulated mesh when the displacements are relatively small. Linear interpolation was used to compute the volume change at all points on the surface between the nodes producing a measure defined continuously on the entire surface.

2.3. Carpal bone segmentation and clinical assessment

Three bones (the capitate, scaphoid and trapezium) were selected for analysis for each patient. Two sets of analyses were conducted. The first was to characterize the segmentation variability and algorithmic stability cross-sectionally and longitudinally when no anatomical change occurred. The second was to characterize longitudinal change by the proposed method and compare with radiological outcome.

2.3.1. Intra-observer variability and algorithmic stability—A board-certified musculoskeletal radiologist noted no clinically significant change for the trapezium from baseline at the 90±7 day follow-up for all four patients. The trapezium was used as a control and was segmented by a single reader 5 times each at two time points with an interval of 1 month between consecutive segmentations. The segmentation was carried out in a semi-automated manner using the BrainSuite software [12]. Specifically, this involved a single step of intensity thresholding, followed by choosing the connected component associated with each selected bone. Dilation and erosion operations were then performed to delineate the bone. The segmentation from baseline was warped to that from follow-up using the method described in section 2.2 and morphometric changes were noted.

2.3.2. Quantification of longitudinal change—Changes in the capitate and scaphoid bone erosion status were classified by the radiologist using three categories, (A) increase in bone erosion (clinical non-responder), (B) decrease in bone erosion (clinical responder), and (C) no change in bone erosion status (clinical responder). The capitate and scaphoid were segmented at baseline and at follow-up for each patient scan as outlined above by a reader who was blinded to the radiological outcome. Morphometric analyses were conducted as described in section 2.2 between the baseline and follow-up imaging data. Outcomes of the 6-month standard-of-care rheumatologist examination were obtained for comparison.

3. RESULTS

3.1. Normal variation in bone erosion status and volume

Figure 4 shows representative surface variations because of repeated segmentation of the trapezium bone at the two time points. In this patient, the average trapezium volume was 1415 mm^3, while the standard deviation over the five measurements was 15 mm^3. When the task was repeated 1 month later, the average trapezium volume was 1414 mm^3, while the standard deviation over the five measurements was 18 mm^3. The same order of repeatability was found for the trapezium bones in the other patients. The change in the point-wise volume change measurement was <0.05 mm^3.

3.2. Changes in erosive status and comparison with radiological and clinical outcome

In two out of the four patients studied, insignificant change based on the normal variation in measurement of the bone erosion metrics was noted. This perfectly correlated with the radiologist assessment and the 6-month rheumatologist examination. In the third patient, continuing erosive changes were detected by the radiologist from CT at follow-up. The results for our method for the scaphoid bone are shown in Fig. 5. A maximum change (decrease) in the point-wise volume change measurement was 0.3 mm^3. The bone volume showed a similar degree of change decreasing from 3325 mm^3 to 3309 mm^3. This patient was indeed found to be a non-responder to the drug at the 6-month clinical examination. In the fourth patient, radiologist interpretation was that there was no change in bone status, however, our analysis showed an increase in the point-wise volume change measurement with a maximum of 0.12 mm^3. The 6-month clinical examination showed that this patient was a responder to the drug.

4. DISCUSSION AND CONCLUSIONS

We have described a method for performing rapid morphometric analysis to localize and quantify erosive changes, or the lack thereof, in patients undergoing therapy for IA. The proposed method was stable and produced satisfactory performance for characterizing normal variation. Our results correlated well with the clinical outcome in this cohort, but there were discordant findings between the radiologist score and the proposed method for

one patient. Since the 6 month follow up showed this patient was responsive, we hypothesize that this may be because the proposed method is more sensitive to change. The current sample size however is clearly inadequate to test this claim. Since this was a proof-of-principle study, it was conducted in a small sample. We expect to continue to validate the technique in future studies and examine metrics at earlier time points (e.g., after 30 days of therapy).

Acknowledgments

This work was funded by the NIH grants P50 AR060752 Pilot Award, R01 CA129561, R03 EB015099 and the UC Davis Vision Grant. The authors would like to acknowledge Dr John C. Hunter, Andrea Ferrero, Dr Kai Yang, and Dr John M. Boone of the UC Davis Department of Radiology for providing image interpretation results and for assistance with data acquisition.

5. REFERENCES

[1]. Brown, M.; Boers, M.; Luqmani, R.; Pincus, T.; Boers, M. Rheumatoid Arthritis. Oxford University Press; New York: 2010. Epidemiology, genetics and economic burden of rheumatoid arthritis; p. 1-9.

[2]. Aubry MC, Maradit-Kremers H, Reinalda M, Crowson C, Edwards W, Gabriel S. Differences in atherosclerotic coronary heart disease between subjects with and without rheumatoid arthritis. Journal of Rheumatology. 2007; vol. 34(no. 5):937–942. [PubMed: 17361987]

[3]. Bathon JM, Martin RW, Fleischmann RM, Tesser JR, Schiff MH, Keystone EC, Genovese MC, Wasko MC, Moreland LW, Weaver AL, Markenson J, Finck BK. A comparison of etanercept and methotrexate in patients with early rheumatoid arthritis. N Engl J Med. 2000; vol. 343(no. 22):1586–93. [PubMed: 11096165]

[4]. Landewe R. The benefits of early treatment in rheumatoid arthritis: confounding by indication, and the issue of timing. Arthritis & Rheumatism. 2003; vol. 48(no. 1):1–5. [PubMed: 12528097]

[5]. Perry D, Stewart N, Benton N, Robinson E, Yeoman S, Crabbe J, McQueen F. Detection of erosions in the rheumatoid hand; a comparative study of multidetector computerized tomography versus magnetic resonance scanning. J Rheumatol. 2005; vol. 32(no. 2):256–267. [PubMed: 15693085]

[6]. Jacq J, Cresson T, Burdin V, Roux C. Performing accurate joint kinematics from 3-d in vivo image sequences through consensus-driven simultaneous registration. Biomedical Engineering, IEEE Transactions on. 2008; vol. 55(no. 5):1620–1633.

[7]. Mattingly P, Matheson J, SON R. The distribution of radiological joint damage in the rheumatoid hand. Rheumatology. 1979; vol. 18(no. 3):142–148.

[8]. Boone JM, Yang K, Burkett GW, Packard NJ, Huang S.-y. Bowen S, Badawi RD, Lindfors KK. An X-Ray computed tomography/positron emission tomography system designed specifically for breast imaging. Technology in Cancer Research & Treatment. 2007; vol. 9(no. 1):29–44.

[9]. Chung, M.; Taylor, J. Diffusion smoothing on brain surface via finite element method. Biomedical Imaging: Nano to Macro, 2004. IEEE International Symposium on. IEEE; 2004. p. 432-435.

[10]. Joshi A, Chaudhari A, Li C, Dutta J, Cherry S, Shattuck D, Toga A, Leahy R. Digiwarp: a method for deformable mouse atlas warping to surface topographic data. Physics in Medicine and Biology. 2010; vol. 55:6197. [PubMed: 20885019]

[11]. Eckstein I, Joshi A, Kuo C, Leahy R, Desbrun M. Generalized surface flows for deformable registration and cortical matching. Medical Image Computing and Computer-Assisted Intervention–MICCAI 2007. 2007:692–700.

[12]. Shattuck DW, Leahy RM. BrainSuite: an automated cortical surface identification tool. Medical Image Analysis. 2002; vol. 6(no. 2):129–142. [PubMed: 12045000]

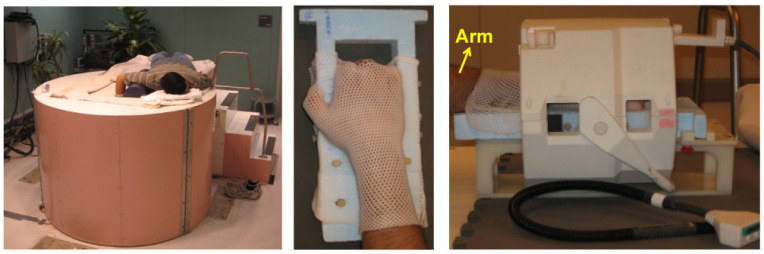

Fig. 1.
High resolution hand imaging; (a) a model on the the UC Davis high resolution extremity CT scanner, (b) the patient-specific thermoplastic immobilizer that was used for longitudinal scanning to improve repositioning, and (c) a patient's hand in the RF coil on a 1.5T MRI scanner.

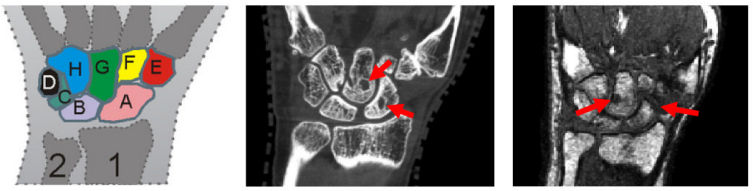

Fig. 2.

Carpal bone destruction in arthritis; (a) the carpal bones of the human hand (Source: Wikipedia). Shown are A=Scaphoid, B=Lunate, C=Triquetral, D=Pisiform, E=Trapezium, F=Trapezoid, G=Capitate, H=Hamate, 1=Radius, 2=Ulna, (b) and (c) representative sections from CT and T_1-weighted MR images respectively of two IA patients showing erosion of the capitate and scaphoid bones.

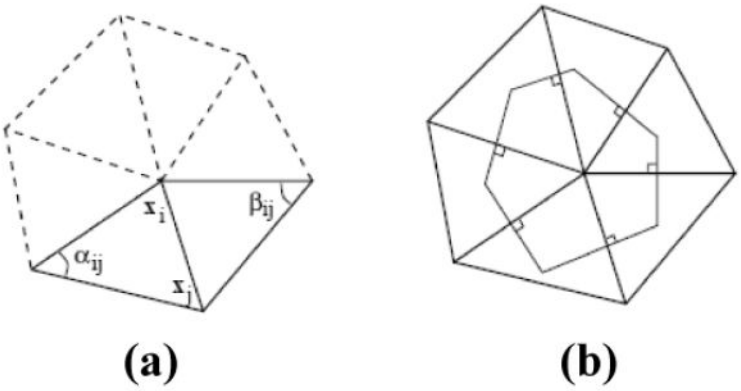

Fig. 3.
Voronoi cell; (a) a triangulated polyhedral surface mesh; (b) Voronoi cell for the vertex *i*.

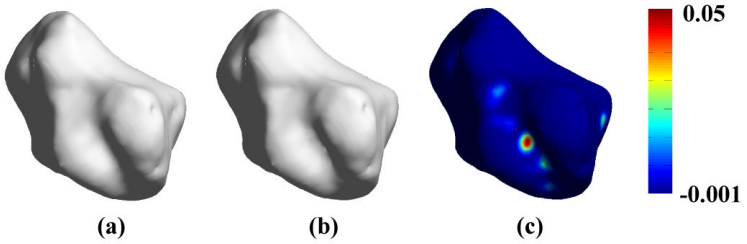

Fig. 4.

Morphometric analysis of the trapezium; (a), (b) surface rendering of the bone at baseline and at follow-up post-therapy respectively, (c) point-wise change map in mm^3 rendered on the surface of the trapezium attributed only to segmentation errors.

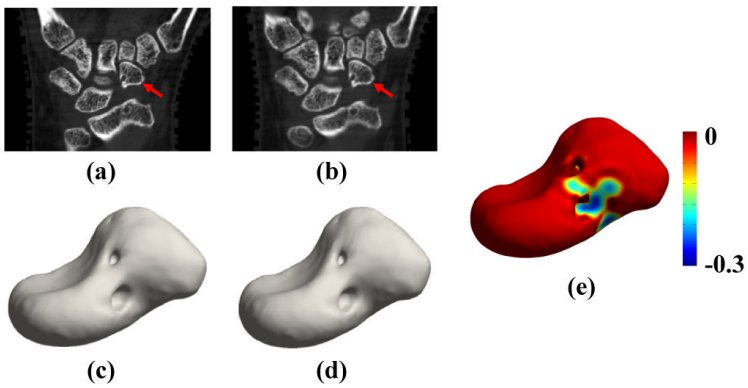

Fig. 5.

Morphometric analysis in the non-responder; (a) CT image of the carpal region at baseline, (b) rigidly co-registered CT image at the ~90 days post-therapy, (c), (d), (e) surface renderings of the scaphoid bone at baseline, follow-up, and the *change* map in mm^3 showing regions of continuing erosion in spite of treatment, respectively.